Cesium Copper Iodide Tailored Nanoplates and Nanorods for Blue, Yellow and White Emission

Parth Vashishtha,[†]* Gautam V. Nutan,[†] Benjamin E. Griffith,[‖] Yanan Fang,[†] David Giovanni,[§] Metikoti Jagadeeswararao,[‡] Tze Chien Sum,[§] Nripan Mathews,[†‡] Subodh G. Mhaisalkar,[†‡] John V. Hanna, [‖†]* Tim White[†]*

[†]School of Materials Science and Engineering, Nanyang Technological University (NTU), 50 Nanyang Avenue, Singapore 639798, Republic of Singapore

[‡]Energy Research Institute @NTU (ERI@N), Research Techno Plaza, X-Frontier Block, Level 5, 50 Nanyang Drive, Singapore 637553, Republic of Singapore

[‖]Department of Physics, University of Warwick, Coventry CV4 7AL, United Kingdom

[§]Division of Physics and Applied Physics, School of Physical and Mathematical Sciences, Nanyang Technological University, 21 Nanyang Link, Singapore, 637371, Republic of Singapore

ABSTRACT: Inorganic metal halide perovskite nanocrystals (NCs) are promising materials for emission-based applications, however, the inclusion of toxic lead may limit their commercial viability. This paper describes two cesium cupriferous iodides as non-toxic alternatives to lead containing perovskites. These nanocrystals were synthesized with tailored composition and morphology by a hot-injection colloidal route to produce hexagonal plates (NPs) of blue-emitting $Cs_3Cu_2I_5$ and nanorods (NRs) of yellow-emitting $CsCu_2I_3$. Phase purity was confirmed by Rietveld refinement of X-ray powder diffraction patterns and solid state ^{133}Cs MAS NMR with both compounds exhibiting high thermal stability suitable for optoelectronic technologies. Phase mixing allows linear tuning of Commission Internationale de l´Eclairage (CIE) coordinates from (0.145, 0.055) to (0.418, 0.541) such that a 1:8 molar ratio of $Cs_3Cu_2I_5$ NPs and $CsCu_2I_3$ NRs yields white emission, while the ^{133}Cs MAS NMR demonstrates that these photophysical effects are not attributed to any changes in the Cu oxidation state.

Introduction

Semiconductor inorganic metal lead halide perovskites nanocrystals (NCs) are promising candidates for lightning applications due to their high photoluminescence (PL) quantum yield, tunable emission through the entire visible region, low processing cost and high thermal stability.[1-3] However, the PL quantum yield in thin films drops significantly due to loss of ligands during film fabrication and the lower exciton binding energy (~ 14-48 meV) of 3-dimensional perovskite structures[4-7] arising from the corner-connectivity of $[PbBr_6]^{4-}$octahedra that promotes fast exciton dissociation.[8-9] Reducing crystallographic dimensions results in larger exciton binding energies and higher performing light emitting diodes (LEDs).[8,10-11] For instance, Saidaminov *et al.*[8] found the PL quantum yield rose from 0.1 % for 3-dimensional $CsPbBr_3$ to 45 % for zero dimensional Cs_4PbBr_6. In the latter, the $[PbBr_6]^{4-}$ octahedra are isolated and physically separated by Cs^+ ions which confines excitons within the octahedra to deliver higher PL quantum yield.[12] Similarly, Zhang *et al.*[13] reported that NCs of Cs_4PbBr_6 show improved optical properties and stability. However, the toxicity of lead (Pb) remains an obstacle for the deployment of plumbous perovskites and related phases.[14] Stannous perovskites have been proposed as a harmless alternative due the presence of lone pair electrons comparable to Pb^{2+}, but Sn^{2+} readily oxides to Sn^{4+} under ambient conditions which destabilises the perovskite.[15-16] Also, $CsSnX_3$ NCs show poor PL quantum yield due to intrinsic crystal defects.[17] Similarly, other Pb-free perovskites such as $Cs_3Bi_2I_9$, $CsSbBr_3$ and $MASnI_3$ (MA=methyl ammonium) are insufficiently efficient and stable.[18-19] Finally, double perovskites including $Cs_2AgInCl_6$, Cs_2AgBiX_6 and $Cs_2AgSbCl_6$ remain unproven for optoelectronic applications.[20-22]

Recently, lead-free $Cs_3Cu_2I_5$ with a zero-dimensional electronic structure has shown excellent blue emission and may be viable for LED applications.[23] Subsequently, Roccanova *et al.*[24] demonstrated 50-98% PL quantum yield in the $Cs_3Cu_2Br_{5-x}I_x$ solid solution and suggested bromination provides relatively higher stability. Li *et al.*[25] reported green emission from $CsCuBr_2$ micro-crosses and demonstrated this material as an active layer in LEDs.[25] Albeit, the bulk properties and synthesis of zero-dimensional $Cs_3Cu_2X_5$ and

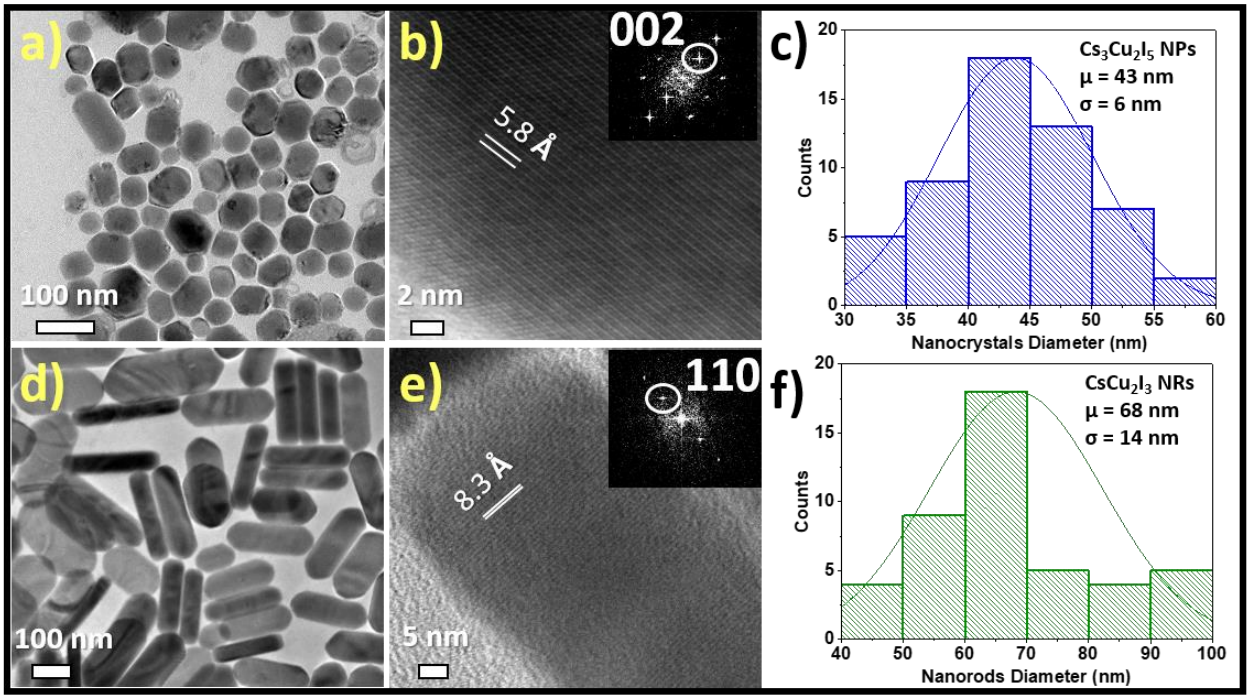

Figure 1. Transmission electron micrographs of a) $Cs_3Cu_2I_5$ Pand d) $CsCu_2I_3$ NRs, including imaging of lattice planes of b) $Cs_3Cu_2I_5$ NPs and e) $CsCu_2I_3$ NRs with inset fast Fourier transform (FFT) images showing the crystallinity and planes of both samples. (c,e) Histograms of particle size, estimated as mean diameter of hexagons and Nanorods, are also included in Table S3.

$CsCu2Br_5$ have been reported but they are yet to be explored in the form of colloidal nanocrystals.[23,25] In addition to $Cs_3Cu_2I_5$, another phase $CsCu_2I_3$ is not reported in the literature.[23] To the best of our knowledge, colloidal NCs of cupriferous perovskites and related phases have never been explored, despite the fact that colloidal chemistry offers superior stability and shape control for NCs through the judicious choice of ligands.

This paper describes the first synthesis of the shape- and composition-controlled $Cs_3Cu_2I_5$ nanoplates (NPs) and $CsCu_2I_3$ nanorods (NRs) with ≥99% purity via a hot-injection colloidal route with functionality adjusted by tailoring the reaction temperature and ligand proportions. $Cs_3Cu_2I_5$ NPs and $CsCu_2I_3$ NRs show blue emission (444 nm) and yellow emission (561 nm) respectively. As $Cs_3Cu_2I_5$ and $CsCu_2I_3$ are pure iodide phases the mixed halide migration observed in perovskites is avoided,[1,26] and therefore, pure white emission was achieved by appropriate mixing of these phases. Solid state ^{133}Cs MAS NMR studies have been introduced to probe the local order and Cs speciation generated within the bulk of each nanocrystal system, and to demonstrated the ability of these systems to fix the Cu speciation in the Cu(I) oxidation state.

Results and Discussion

Synthesis. Colloidal NCs were synthesized a hot-injection route where Cs-oleate was injected into a hot reaction mixture of copper(I) iodide, 1-octadecene, oleic acid and oleylamine at 100-160 °C under an inert atmosphere. The nanocrystals were grown for ~10 s at high temperature before rapid cooling in an ice bath. As-synthesized NCs were twice purified by solvent/antisolvent cycles before re-dispersion in anhydrous hexane. Phase purity and crystal morphology were controlled by varying the reaction temperature, ligand proportion, and precursor concentration (see Experimental for details). It should be noted that the shape control could not be precisely achieved by changing the growth time since the growth rate of nanocrystals were very fast therefore it was achieved by changing the reaction temperature.

Crystallochemical Properties. By controlling the reaction conditions cesium copper iodide can crystallize as either $Cs_3Cu_2I_5$ or $CsCu_2I_3$. When synthesized at 110°C $Cs_3Cu_2I_5$ appears as hexagonal NPs with average diameter of ~ 43 nm, while $CsCu_2I_3$ crystallizes as NRs with average diameter of ~ 68 nm and average length of ~201 nm (Figure 1, Figure S9). Low-resolution SEM images for both materials are shown in Figure S8. Changing reaction temperature did not result in smaller particles. Instead, NPs of variable shapes result (Figure S7). High-resolution transmission electron microscope (HR-TEM) and fast Fourier transformation (FFT) (Figure 1b and 1d) confirmed the crystal perfection of both phases. As expected, the XRD reflections for the $Cs_3Cu_2I_5$ NPs were broadened compared to the bulk material (Figure 2).[27-28] Rietveld refinement using TOPAS confirmed phase pure (≥99%) orthorhombic lattices of $Cs_3Cu_2I_5$ (*Pnma*) and $CsCu_2I_3$ (*Cmcm*) and lattice parameters of a= 10.1720(4) Å, b= 11.6497(4) Å, and c= 14.3556(5) Å, and a= 10.5470(1) Å, b= 13.1732(2) Å, and c= 6.0967(2) Å respectively. The TEM lattice fringes of d-spacing ~5.8 Å and ~8.3 Å (Figure 1b, 1e) are consistent with the (002) and (110) planes of $Cs_3Cu_2I_5$ and $CsCu_2I_3$. Additionally, energy-dispersive X-ray spectroscopy (EDXS) yielded Cs:Cu:I average molar ratios of 2.94:2.00:5.62 in $Cs_3Cu_2I_5$ NPs and 1.02:2.00:3.50 in $CsCu_2I_3$ NRs (Table S1 and S2) in good

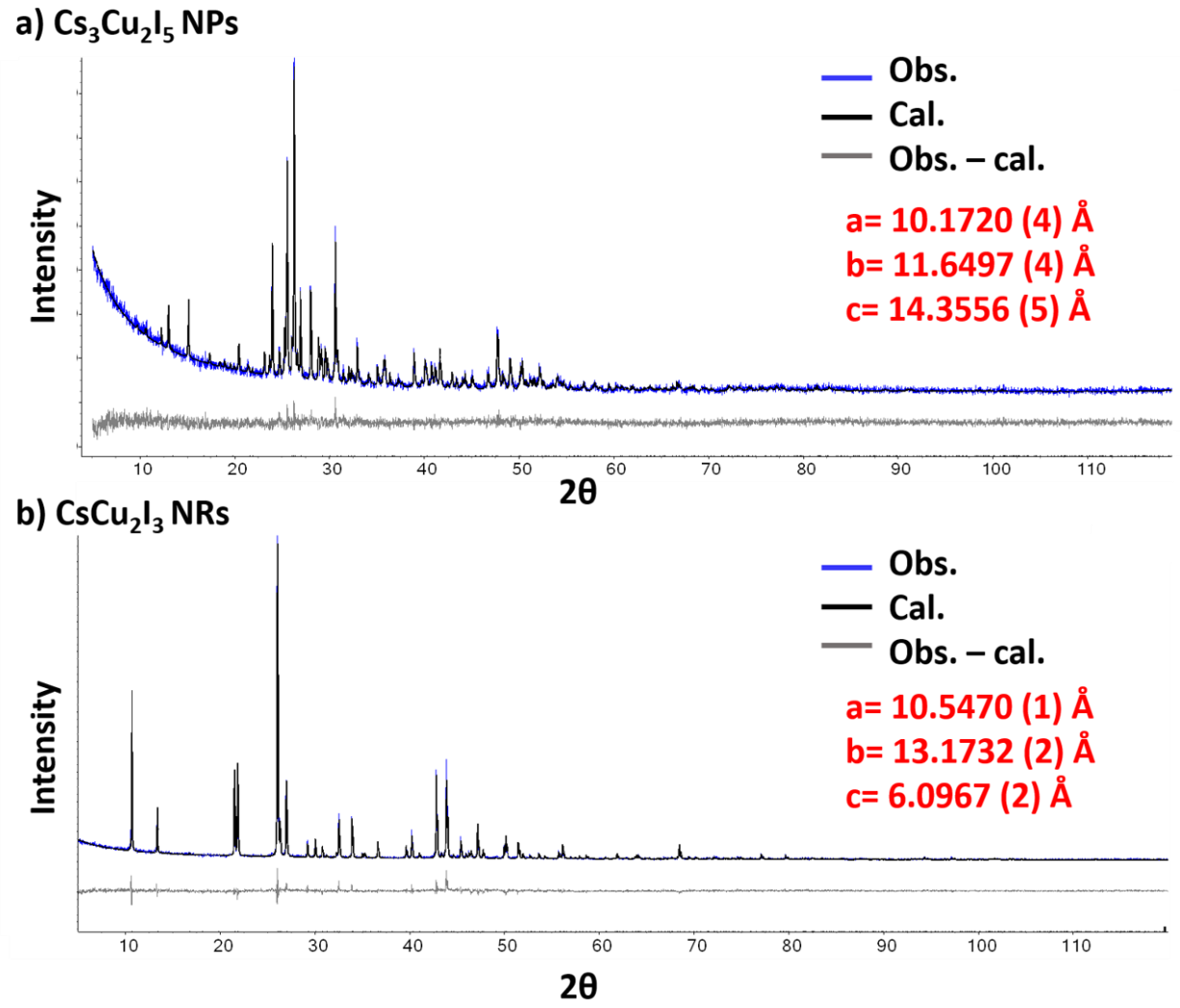

Figure 2. Powder XRD patterns (blue lines) of (a) $Cs_3Cu_2I_5$ NPs and (b) $CsCu_2I_3$ NRs with structural refinements fits (black line) using TOPAS and residual map of both graphs (gray).

agreement with the anticipated composition. Moreover, XPS elemental analysis, presented in Table S5, yields even accurate molar ratio of 2.90:2.05:5.15 in $Cs_3Cu_2I_5$ NPs and 0.92:2.04:2.91 in $CsCu_2I_3$ NRs.

$Cs_3Cu_2I_5$ is a zero dimensional structure containing Cu^+I_4 tetrahedra and a Cu^+I_3 triangles that are edge-connected to form isolated $[Cu_2I_5]^-$ units separated by Cs^+ ions in Wyckoff positions 4c [0.5948(5), ¼, 0.5506(4)] and 8d [0.0524(4), 0.9897(4), 0.6783(2)] (Figure 3a).[23-24] $CsCu_2I_3$ has one dimensional morphology where edge-sharing and face-sharing Cu^+I_4 tetrahedra form infinite double chains of composition of Cu_2I_3 interspersed by cesium in the 4c Wyckoff position [0, 0.6722(2), 1/4] (Figure 3b). Refined atomic positions for $Cs_3Cu_2I_5$ NPs and $CsCu_2I_3$ NRs are listed in Table S4 and S5. Both phases are stable under ambient conditions with insignificant degradation observed by XRD over two months (Figure S4).

Here, oleylamine/oleic acid ligands were used exclusively as reconnaissance investigations with branched chain 2-hexyldecanoic acid as the organic ligand failed to improve structural properties and nanocrystal size (Figure S5). Moreover, 2-hexyldecanoic acid caused the poor colloidal suspension of $CsCu_2I_3$ NRs in hexane due to poor ligand passivation on NR surfaces (Figure S5).

The solid state ^{133}Cs MAS NMR data from the $Cs_3Cu_2I_5$ and $CsCu_2I_3$ systems is shown Figure 4. For the $Cs_3Cu_2I_5$ a variation of the MAS frequency (from 8 - 12 kHz) allows a clear identification of the ^{133}Cs chemical shifts associated with this structure. From Figures 4a and 4b relating to the bulk $Cs_3Cu_2I_5$ crystals, and from Figures 4c and 4d from the $Cs_3Cu_2I_5$ NPs, two ^{133}Cs resonances can be observed at the well-defined shifts of 130.0 and –13.6 ppm. These shifts correspond to the two distinct Cs positions (4c and 8d) in the $Cs_3Cu_2I_5$ orthorhombic *Pnma* unit cell. In contrast, from Figure 4e for the $CsCu_2I_3$ NRs system (orthorhombic unit cell *Cmcm*), only one ^{133}Cs chemical shift at is observed at –51.6 ppm which coincides with the single Cs 4c position in this structure. Of particular note from these ^{133}Cs MAS NMR data is the high quality of the $Cs_3Cu_2I_5$ NPs and $CsCu_2I_3$ NRs systems produced (see Figures 4c, 4d and 4e), which are comparable to the quality of the bulk preparation. These data demonstrate that the hot-injection

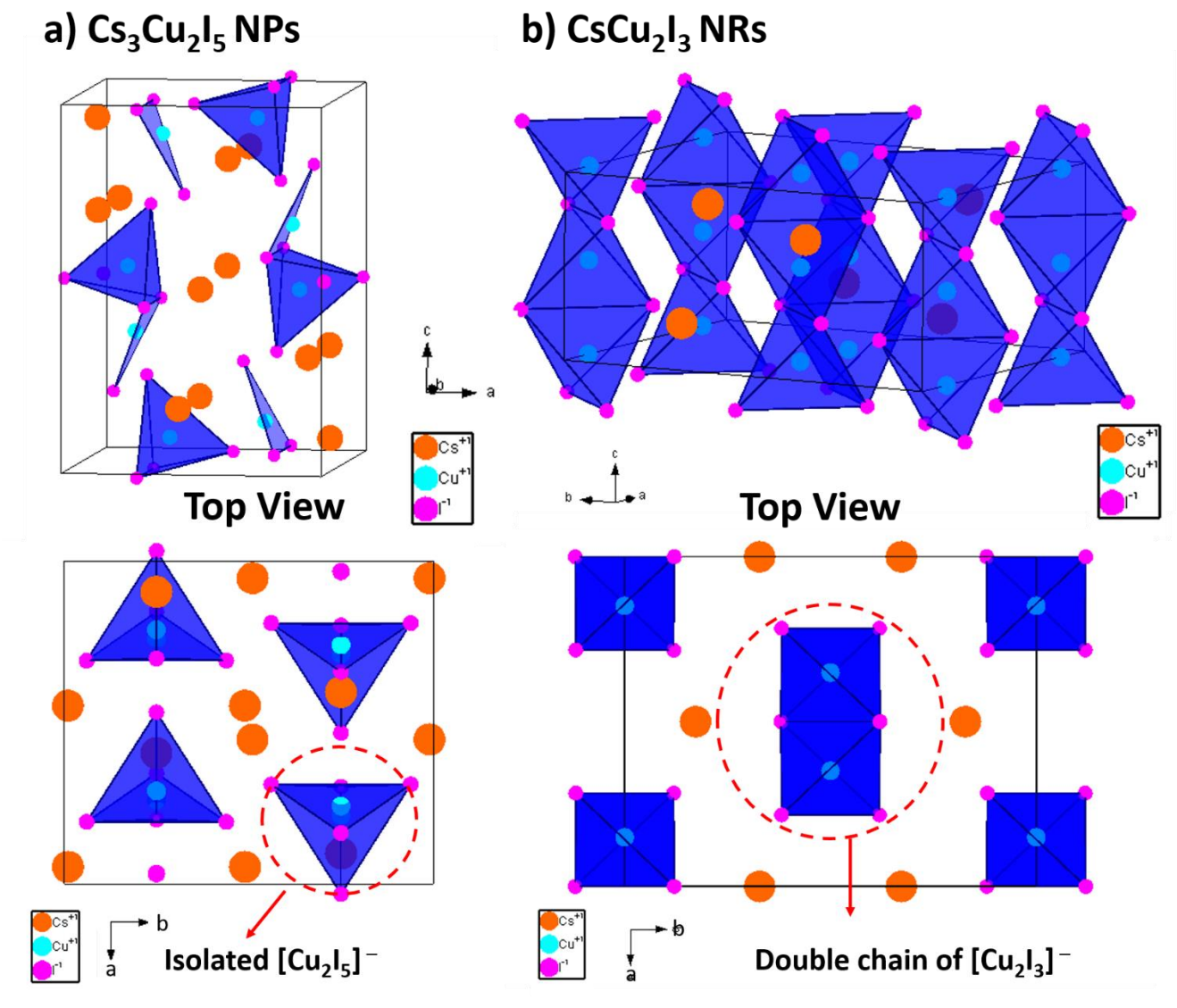

Figure 3. Crystal structure of (a) $Cs_3Cu_2I_5$ NPs and (b) $CsCu_2I_3$ NRs with optimized lattice parameters. A top view of $Cs_3Cu_2I_5$ crystal shows the isolated $[Cu_2I_5]^-$. Similarly, $CsCu_2I_3$ structure shows the double chains of $[Cu_2I_3]^-$ from top view.

method (with the associated optimized parameters and precursor quantities) used in the synthesis of the $Cs_3Cu_2I_5$ and $CsCu_2I_3$ systems yields phase pure materials and very high quality NCs. In addition, the $Cs_3Cu_2I_5$ system is the more energetically favorable phase, so with the correct optimization of the synthesis conditions high quality bulk material can also be produced. Furthermore, the clarity of these high resolution ^{133}Cs data demonstrates that no paramagnetic broadening and/or shift is experienced in these systems, thus suggesting that the Cu(I) oxidation state is predominant throughout the bulk of each particle.

The combination of TEM, EDXS and XRD with NMR unequivocally confirm the formation of $Cs_3Cu_2I_5$ NPs and $CsCu_2I_3$ NRs. However, to validate copper speciation X-ray photoelectron spectroscopy (XPS) was conducted (Figure 5a). For both phases, the copper binding energies of 952.3 eV and 932.4 eV for $2p^{1/2}$ and $2p^{3/2}$ respectively confirms that copper is overwhelmingly monovalent and consistent with NMR results.[29] Oxidation states for Cs and I are also consistent with the corresponding materials as depicted in Figure S1. High thermal stability is essential for optoelectronic device applications. For instance, cupriferous hybrid organic-inorganic metal halide compounds such as zero-dimensional $[N(C_2H_5)_4]_2Cu_2Br_4$ and one-dimensional $(C_8H_{14}N_2)_2Cu_2Br_6$ and $CH_3NH_3Cu_2I_3$ can be phase pure but possess poor thermal stability due to an organic component on the A cation site.[30-32] TGA of 2-times purified and dried (see Experimental) $Cs_3Cu_2I_5$ NPs and $CsCu_2I_3$ NRs found that weight loss up to 450 °C could be accounted for by the removal of ligands (Figure 5b). $Cs_3Cu_2I_5$ NPs show significant loss at 670 °C, while $CsCu_2I_3$ NRs degraded at 610 °C. Overall, both materials show thermal stability exceeding hybrid organic-inorganic perovskites.

Optical Properties. $Cs_3Cu_2I_5$ NPs have strong excitonic absorption at 286 nm and blue emission at 444 nm with a broad FWHM of 79 nm (Figure 6a), which is consistent with previous reports for $Cs_3Cu_2I_5$ thin films and single crystals.[23] Similarly, $CsCu_2I_3$ NRs display yellow emission at

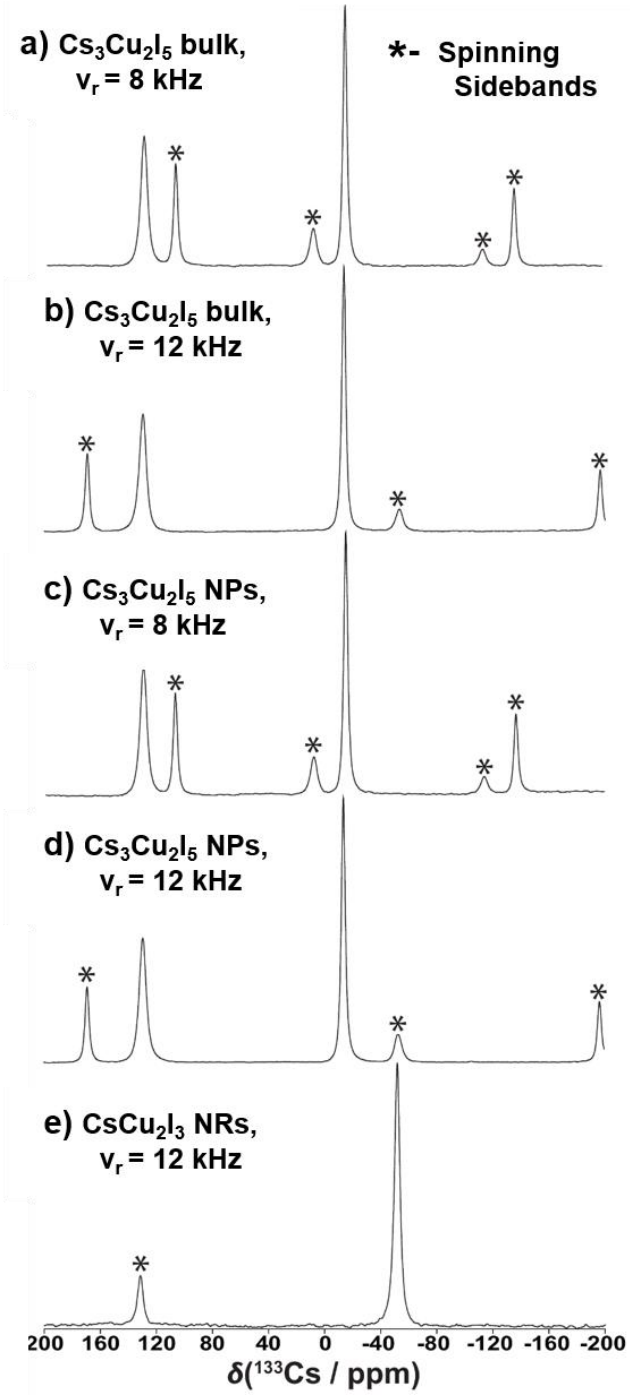

Figure 4. The solid state ^{133}Cs MAS NMR spectra of (a) $Cs_3Cu_2I_5$ bulk at 8 kHz, (b)$Cs_3Cu_2I_5$ bulk at 12 kHz, (c) $Cs_3Cu_2I_5$ NPs at 8 kHZ, (d) $Cs_3Cu_2I_5$ NPs at 12 kHz, and (e) $CsCu_2I_3$ NRs at 12 kHz.

561 nm with strong excitonic absorption at 321 nm. For both materials, 3D emission spectra show no peak shift invoked by changing the excitation wavelength (Figure S3) confirming the absence of mixed phases. Absorption spectra show sharp edges at 284 nm for $Cs_3Cu_2I_5$ NPs and 321 nm for $CsCu_2I_3$ (Figure S2) indicating that the PLE is due to the excitonic absorption.[33] $Cs_3Cu_2I_5$ NPs and $CsCu_2I_3$ NRs have long carrier lifetimes of approximately 1.1 µs and 0.1 µs respectively (Figure 6b). Using Tauc plots, the band gaps of $Cs_3Cu_2I_5$ NPs and $CsCu_2I_3$ NRs were found to be 4.1 eV and 3.6 eV respectively, which was slightly larger than the bulk materials (Figure 6c).[23,34] A large Stokes shift is consistent with previous studies.[23-24] This suggests emission is not from the direct bandgap, but most likely due to self-trapped excitons which originate either from the Jahn-Teller distortion or strong exciton-phonon coupling.[24,35] Jun *et al.*[23,36] observed similar behavior in $Cs_3Cu_2I_5$ polycrystalline thin films and suggested that the emission mechanism arises from excited state structural reorganization as a result of Jahn-Teller distortion.[23,36] Tetrahedral Cu(I)-d10 forms a Cu(II)-d^9 photoexcited state (Figure S6). Typically, Cu(II) undergoes strong Jahn-Teller distortion since the e_g orbital is asymmetrical filled in d^9 center Therefore, the energy difference between Cu(I)- d10 and Cu(II)- d^9 is responsible for a large

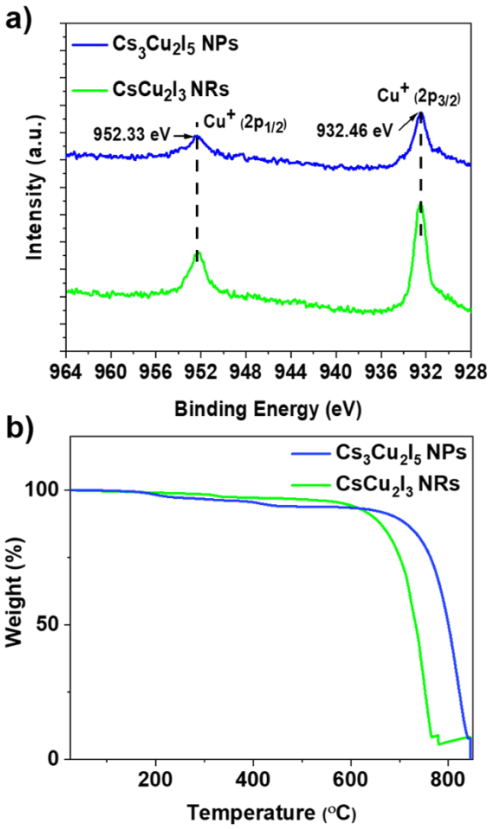

Figure 5. (a) Cu XPS spectra of $Cs_3Cu_2I_5$ NPs (Blue) and $CsCu_2I_3$ NRs (green) showing the valency of Copper. **(b)** TGA plots of both samples showing the thermal stability for $Cs_3Cu_2I_5$ NPs (Blue) and $CsCu_2I_3$ NRs (green).

Stokes shift.[23] However, Roccanova *et al.* proposed the self-trapped exciton mechanism due to the exciton-photon coupling. Similar large Stoke shifts as a result of Jahn-Teller

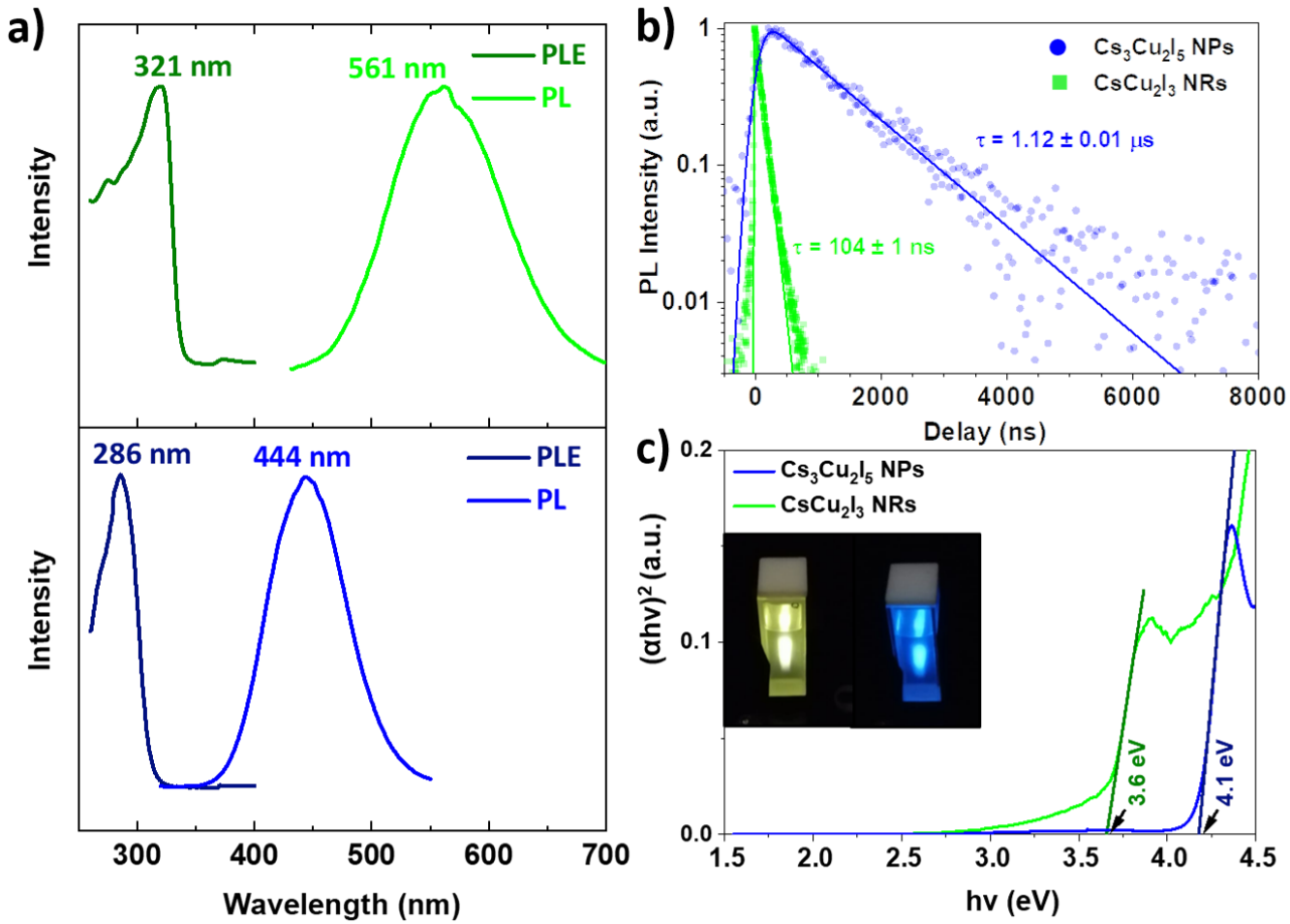

Figure 6. (a) PL excitation and emission spectra of NCs solution in hexane showing excitation peak at 286 nm and 321 nm and emission peak at 444 nm and 561 nm for $Cs_3Cu_2I_5$ NPs (Blue) and $CsCu_2I_3$ NRs (green), respectively. (b) Time-resolved PL decay kinetics for both samples at their emission peaks. (c) Tauc plot for both samples showing the band gap of 4.1 eV for $Cs_3Cu_2I_5$ NPs and 3.6 eV for $CsCu_2I_3$ NRs, with photographs of these samples in hexane excited by UV lamp.

distortion was observed in other perovskite and related-materials, such as $Cs_2Ag_xNa_{1-x}InCl_6$, $C_4N_2H_{14}PbBr_4$, $(C_4N_2H_{14}X)_4SnX_6$ and $(C_9NH_{20})_2SbX_5$.[35,37-38] However, a detailed excited state structural analysis is required to verify that Jahn-Teller effects are operating. The PL quantum yields (PLQY) were ~35% for $Cs_3Cu_2I_5$ NPs and 11% for $CsCu_2I_3$ NRs at low excitation power densities of 0.20 μJ/cm² and 0.57 μJ/cm² respectively. These values are comparable to observations of perovskites where higher excitation power densities were employed.[39-40] The PLQY of $Cs_3Cu_2I_5$ nanoplates are lower than the bulk sample reported in literature.[23] This can be attributed to the fact that surface defects in nanocrystals are responsible for nonradiative surface recombination as a result of higher surface to volume ratio in nanocrystals. The broad emission profile is due the phosphorescent emission from Cu(I)-complexes.[41-42] Most likely, the higher exciton binding energy in zero-dimensional $Cs_3Cu_2I_5$ NRs results in the higher PLQY.[8,23] No notable decrease in relative PLQY was observed even after 2 months under ambient conditions. The stable emission properties of this material along with the high PLQY makes $Cs_3Cu_2I_5$ a promising candidate for absorption and emission applications such as solid-state lightning, UV photo detectors, X-ray detection and light emitting diodes.[23]

As $Cs_3Cu_2I_5$ NPs and $CsCu_2I_3$ NRs are pure iodides the halide ion segregation observed in $CsPb(Br/I)_3$ is avoided.[1,26] For instance, when pure $CsPbBr_3$ NCs with characteristic emission at ~518 nm is mixed with pure $CsPbI_3$ NCs with emission at 690 nm homogenization to $CsPb(Br_{0.50}/I_{0.50})_3$ leads to emission at ~600 nm.[43] This is a major obstacle to producing white light from lead-halide 3D perovskites, since the white emission is the combination of blue, green, and red emission. $Cs_3Cu_2I_5$ NPs and $CsCu_2I_3$ NRs have significant blue, green and red components and mixing them in an appropriate ratio (1:8) produces white emission from these NCs (Figure 7). To our knowledge, this is the first instance of Commission Internationale de l´Eclairage white light emission (CIE: 0.290, 0.311) from copper based materials (Figure 7b). Additionally, linear tuning in CIE coordinates is possible by mixing $Cs_3Cu_2I_5$ NPs and $CsCu_2I_3$ NRs in different proportions (Figure 7a) as illustrated by irradiation under a 307 nm UV lamp (Figure 7c). Overall, a combination of these two materials can be a potential candidate for lead-free perovskite white LEDs and white luminescent display.

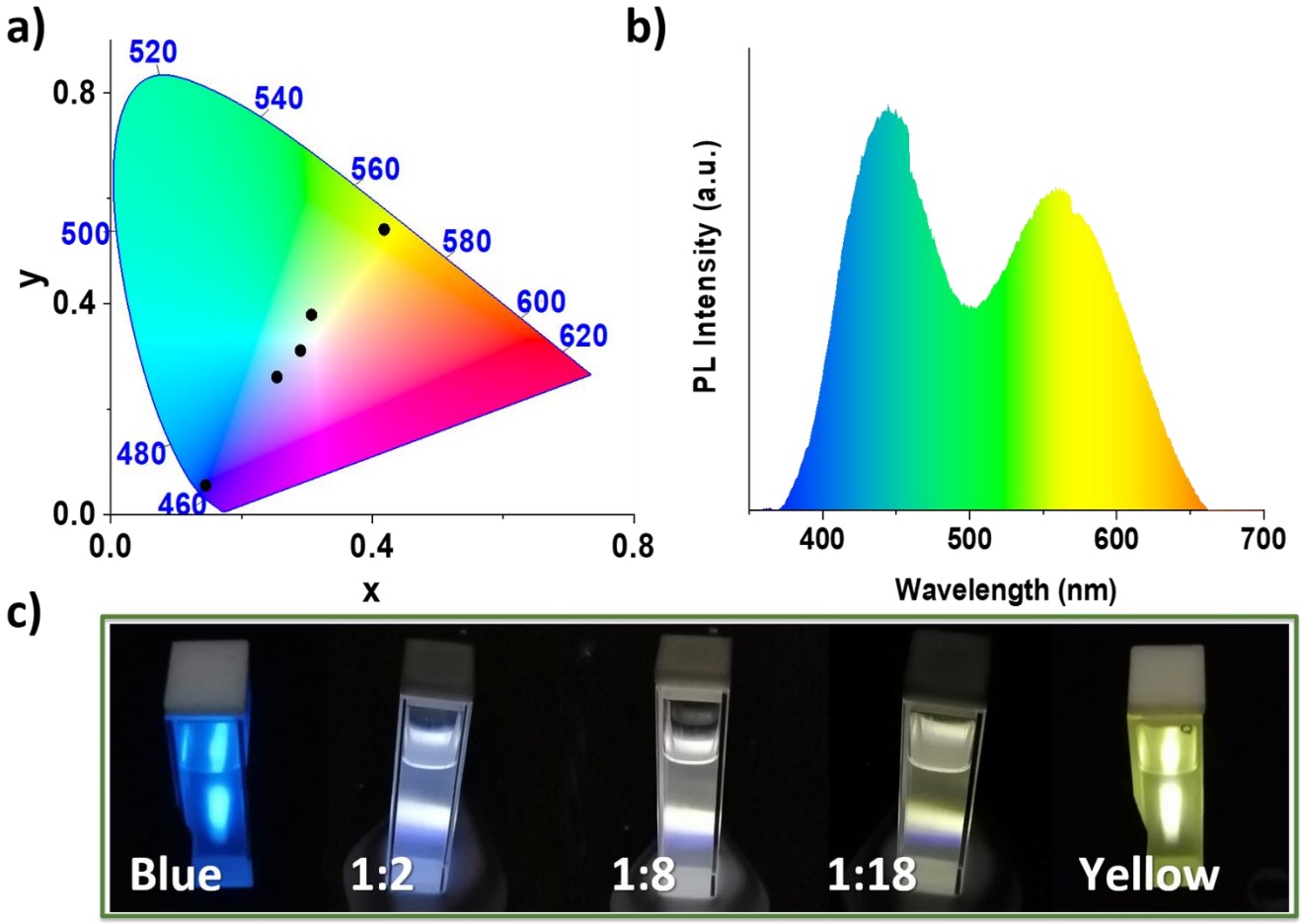

Figure 7. Application of these nanocrystals as a white light emitter. (a) A CIE 1931 graph of these samples showing the linear color tuning from (0.145, 0.055) to (0.418, 0.541) in CIE coordinates. (b) A PL spectrum of white light as a result of mixing $Cs_3Cu_2I_5$ NPs and $CsCu_2I_3$ NRs in 1:8 molar ratio. (c) Photographs of all these mixed samples in hexane excited by UV lamp at 307 nm.

Conclusion

For the first time phase pure (≥99%) colloidal Cs3Cu2I5 NPs and CsCu2I3 NRs have been synthesized by a hot-injection method. Crystal chemical refinements of powder XRD data of Pnma Cs3Cu2I5 and Cmcm CsCu2I3 confirm the composition, symmetry and purity in these crystals that also exhibit high thermal stability. Cs3Cu2I5 NPs and CsCu2I3 NRs display blue (444 nm) and yellow (561 nm) emission respectively. The tunability of emission, including white emission, achieved by mixing these compounds in various ratios may prove applicable for lightning applications.

Experimental

Chemicals and Synthesis:

Chemicals. Cesium carbonate (reagent Plus, 99%), copper(I) iodide (Purum, ≥99.5%), 1-octodecene (technical grade, 90%), oleylamine (technical grade, 70%), oleic acid (90%), 2-hexyldecanoic acid (96%), N,N-Dimethylformamide (anhydrous, 99.8 %), toluene (anhydrous, 99.8 %) and hexane (anhydrous, 95%) were purchased from Sigma-Aldrich.

Synthesis of Cesium Oleate. Synthesis of cesium-oleate was adapted from the literature[44], where 0.81 gm of cesium carbonate, 2.5 ml of oleic acid and 40 of ml 1-octadecene were loaded in a 100 mL 3-neck round bottom flask. The reaction mixture was degassed under vacuum at 100 °C for about an hour followed by heating in nitrogen atmosphere at 150 °C for 30 min. Cesium-oleate solution was transferred in a Schlenk tube with an air-free transfer technique and stored inside a nitrogen-filled glove box until further use. It is noted that Cs-oleate precipitates out from 1-octadecene at room temperature and was heated at 100 °C before hot-injection.

Synthesis of $Cs_3Cu_2I_5$ NPs. 1.22 mmol of CuI was loaded into a 3-neck round bottom flask with 15 mL of 1-octadecene. The mixture was degassed under vacuum at 100 °C for ~1 h. Simultaneously, 3 mL of oleic acid and 3 mL of oleylamine were dried under vacuum at 60 °C. After degassing of reaction mixture, oleic acid and oleylamine were injected to the reaction flask under nitrogen. The temperature was raised to 110 °C and 7.2 mL of Cs-oleate injected into the reaction flask. NPs were grown for 10 s at 110 °C and then the reaction flask was cooled in an ice-water bath.

Synthesis of $CsCu_2I_3$ NRs. The synthesis of $CsCu_2I_3$ NRs was similar to $Cs_3Cu_2I_5$ NPs. However, phase and composition were adjusted through temperature tuning along with precursor and ligand concentration. 0.75 mmol of CuI was loaded into a 3-neck round bottom flask with 15 mL of 1-octadecene. This mixture was degassed under vacuum at 100 °C for ~ 1 h. Simultaneously, 2 mL of oleic acid and 2 mL of oleylamine were dried under vacuum at 50 °C for 60 min, and after degassing, the oleic acid and oleylamine were injected into the reaction flask under nitrogen. The temperature was raised to 160 °C, and 0.8 mL of Cs-oleate injected in the reaction vessel. NRs were grown for 10 s at 160 °C before cooling in an ice-water bath.

Purification of the $Cs_3Cu_2I_5$ NPs and $CsCu_2I_3$ NRs. Purification for both materials was similar. The growth solution was first centrifuged at 10,000 rpm for 12 min. The supernatant was discarded and the solids dispersed in 4 mL of anhydrous hexane followed by centrifuging at 10,000 rpm for 12 min. The resulting precipitate was re-dispersed in 4 mL of anhydrous hexane followed by filtration of the NCs solution using a 0.22 µL PTFE filter.

Synthesis of $Cs_3Cu_2I_5$ Bulk. A bulk sample was synthesized by first preparing the precursor solution in polar solvent. Copper(I) iodide (0.2 mmol) and cesium iodide (0.3 mmol) were dissolved in 1 mL DMF inside a nitrogen-filled glove box. After that, 200 µL of as prepared precursor solution was added in 5 mL of toluene under vigorous stirring. The precipitate was collected by centrifugation at 10,000 rpm for 10 min.

Characterization:

Transmission Electron Microscopy. A JEOL 2010 was used for the HR-TEM analyses at an accelerating voltage of 200 kV and beam current of 106 µA. Samples were prepared by dispersing NPs and NRs in hexane followed by sonication for two minutes and collection on holey carbon support grids.

Scanning Electron Microscopy. SEM measurements were conducted using a JEOL 7600 FESEM at operating at 20 kV. For each sample, a portion of the nanocrystals suspension in hexane was drop cast on ITO coated glass.

Thermal Gravimetric Analysis. TGA measurements were conducted using a TA Q500 instrument. Purified $Cs_3Cu_2I_5$ NPs and $CsCu_2I_3$ NRS were vacuum-treated in order to get dry powder. In each measurement, 10-20 mg of dry powder were placed in alumina crucibles supported by a platinum pan. Samples were measured under nitrogen from room temperature to 800 °C at the ramp rate of 10 °C/min.

X-ray Photoelectron Spectroscopy. XPS measurements were performed using an AXIS Supra spectrometer (Kratos Analytical, UK) equipped with a hemispherical analyser and a monochromatic Al K-alpha source (1487 eV) operating at 15 mA and 15 kV. The XPS spectra were acquired from an area of 700 x 300 µm with a take-off angle of 90°. These measurements were undertaken on solid powder samples pressed on carbon tape. A 3.1-volt bias was applied to the sample to neutralise charge build up on the sample surface. Pass energies of 160 eV and 20 eV were used for survey and high-resolution scans, respectively. The binding energies (BEs) were charge-corrected based on the C 1s at 284.8 eV. To remove the contribution of Cs MNN Auger peaks, high-resolution spectroscopy was also performed for Cu 2p (BE of 865.6 eV to 962.6 eV) with an Ag L-alpha source (2984.2 eV) operated at 25 mA and 15 kV with a pass energy of 80 eV. Quantitative analysis was performed using ESCApe.

X-ray Diffraction. All XRD data were accumulated using a PANalytical X-ray diffractometer equipped with a Cu Kα X-ray tube operating at 40 kV and 30 mA. These diffraction patterns were acquired in air at room temperature using Bragg-Brentano geometry. All XRD samples were prepared by drop casting a concentrated solution on a zero diffraction silicon holder.

Solid State ^{133}Cs Magic-Angle-Spinning (MAS) NMR. Single pulse ^{133}Cs MAS NMR measurements were performed at 11.74 T using a Bruker Avance III-500 spectrometer operating at a Larmor frequency (ν_0) of 65.6 MHz. These experiments were performed using a Bruker 4 mm HX probe enabling MAS frequencies of 8 - 12 kHz to be adopted. Pulse calibration was performed on solid CsCl from which a 'non-selective' (solution) $\pi/2$ pulse time of 4.5 µs was calibrated which corresponded to a 'selective' (solid) $\pi/2$ pulse time of ~1.12 µs on the ^{133}Cs nucleus (I = 7/2). All measurements were undertaken with a 'selective' $\pi/2$ flip angle (~1.12 µs) along with a relaxation delay of 60 s, and all ^{133}Cs chemical shifts were reported against the IUPAC recommended primary reference of 0.1M $CsNO_3$ (aq) (δ_{iso} = 0.0 ppm), via a solid CsCl secondary reference at δ_{iso} = 18 ppm.[45]

UV-Vis Spectroscopy. The absorption spectra were performed on a Cary 5000 UV-Vis-NIR spectrophotometer. Each sample was prepared by diluting the 2nd precipitator solution in hexane in 1 cm path length quartz cuvettes.

Photoluminescence (PL) Measurements. All PL measurements were undertaken using a Cary Eclipse spectrophotometer. Samples were prepared by diluting the NPs or NRs solution in hexane. A quartz cuvette with a path length of 1 cm was used to enable each measurement.

PL Quantum Yield Measurements. All PL measurements were undertaken using a Cary Eclipse spectrophotometer. Samples were prepared by diluting the NPs or NRs solution in hexane. A quartz cuvette with a path length of 1 cm was used to enable each measurement. The PL QY was performed using a femtosecond laser system. The fundamental laser used was a Coherent LIBRA™ with output wavelength of 800 nm, 1 kHz repetition rate and 50 fs pulse-width. This fundamental was sent to Coherent OPeRa Solo™ optical parametric amplifier (OPA), to generate tunable wavelength output from 300 - 2600 nm. In these experiments, 310 nm or 325 nm output was used as the excitation source for $Cs_3Cu_2I_5$ and $CsCu_2I_3$ respectively. The PLQY was measured by using a BaS-coated ø15-cm integrating sphere. The sample was placed in the middle of the integrating sphere, before photoexcited by the laser. The pump scattering and PL from the sample and solvent were collected using an optical fibre attached to the sphere, before sent into a monochromator and CCD for

spectrally resolved measurement. The PLQY was calculated by using the following formula:

$$\text{PL QY} = \frac{\int_{\lambda_{PL1}}^{\lambda_{PL2}} d\lambda\, S(\lambda)\left[I_{\text{sample}}(\lambda) - I_{\text{solvent}}(\lambda)\right]}{\int_{\lambda_{pump1}}^{\lambda_{pump2}} d\lambda\, S(\lambda)\left[I_{\text{solvent}}(\lambda) - I_{\text{sample}}(\lambda)\right]}$$

Here, $S(\lambda)$ is the instrument spectral response function; $I_{solvent}$ and I_{sample} are the collected spectra for the solvent and sample, respectively; $[\lambda_{PL1}, \lambda_{PL2}]$ and $[\lambda_{pump1}, \lambda_{pump2}]$ are the spectral region for the sample PL and the pump, respectively. In order to conduct the relative PL QY over time, absorption normalized PL spectra were used.

Lifetime Measurements. The PL lifetime was measured by first collecting the PL using a lens pair, before directing the emission towards a Princeton Instrument SP2360i™ monochromator coupled with Optronis™ streak camera. This yielded time- and spectrally- resolved PL spectra.

ASSOCIATED CONTENT

Supporting Information

Cs, Cu, and I XPS spectra; absorption spectra; excitation dependent PL spectra; XRD of both samples after 2 months, XRD, PL and PLE of 2-HAD based NCs; Schematic representation of self-trapped exciton mechanism; TEM micrographs of $Cs_3Cu_2I_5$ synthesized at 70 °C; SEM images of NCs; histogram for NRs length; EDXS table for elemental analysis; table for particle size; and optical properties; and table for refined atomic coordinates and XPS elemental analysis for both materials are included in SI.

AUTHOR INFORMATION

Corresponding Author

PVashishtha@ntu.edu.sg
j.v.hanna@warwick.ac.uk
TJWhite@ntu.edu.sg

Notes

The authors declare no competing financial interests.

ACKNOWLEDGMENTS

PV acknowledges a Presidential Postdoctoral Fellowship from Nanyang Technological University (NTU), Singapore via grant M408070000. TCS and DG acknowledge the support from the Ministry of Education Tier 2 grants MOE2017-T2-1-001 and MOE2017-T2-2-002. Access to the NTU shared Facility for Analysis Characterization Testing & Simulation (FACTS) enabled TEM, XRD and XPS measurements. We thank Sai S. H. Dintakurti for valuable discussion on structural analysis, and also acknowledge Dr Teddy Salim for collecting XPS data.

REFERENCES

1. Vashishtha, P.; Halpert, J. E., Field-driven ion migration and color instability in red-emitting mixed halide perovskite nanocrystal light-emitting diodes. *Chemistry of Materials* **2017,** *29* (14), 5965-5973.
2. Sutton, R. J.; Eperon, G. E.; Miranda, L.; Parrott, E. S.; Kamino, B. A.; Patel, J. B.; Hörantner, M. T.; Johnston, M. B.; Haghighirad, A. A.; Moore, D. T., Bandgap-tunable cesium lead halide perovskites with high thermal stability for efficient solar cells. *Advanced Energy Materials* **2016,** *6* (8), 1502458.
3. Dutta, A.; Behera, R. K.; Pal, P.; Baitalik, S.; Pradhan, N., Near-Unity Photoluminescence Quantum Efficiency for All $CsPbX_3$ (X= Cl, Br and I) Perovskite Nanocrystals: A Generic Synthesis Approach. *Angewandte Chemie* **2019,** 131(17), 5608-5612.
4. Manser, J. S.; Kamat, P. V., Band filling with free charge carriers in organometal halide perovskites. *Nature Photonics* **2014,** *8* (9), 737.
5. Miyata, A.; Mitioglu, A.; Plochocka, P.; Portugall, O.; Wang, J. T.-W.; Stranks, S. D.; Snaith, H. J.; Nicholas, R. J., Direct measurement of the exciton binding energy and effective masses for charge carriers in organic–inorganic tri-halide perovskites. *Nature Physics* **2015,** *11* (7), 582.
6. Cha, J.-H.; Han, J. H.; Yin, W.; Park, C.; Park, Y.; Ahn, T. K.; Cho, J. H.; Jung, D.-Y., Photoresponse of CsPbBr3 and Cs_4PbBr_6 perovskite single crystals. *The journal of physical chemistry letters* **2017,** *8* (3), 565-570.
7. Huang, Y.; Yin, W.-J.; He, Y., Intrinsic point defects in inorganic cesium lead iodide perovskite $CsPbI_3$. *The Journal of Physical Chemistry C* **2018,** *122* (2), 1345-1350.
8. Saidaminov, M. I.; Almutlaq, J.; Sarmah, S.; Dursun, I.; Zhumekenov, A. A.; Begum, R.; Pan, J.; Cho, N.; Mohammed, O. F.; Bakr, O. M., Pure Cs_4PbBr_6: highly luminescent zero-dimensional perovskite solids. *ACS Energy Letters* **2016,** *1* (4), 840-845.
9. Yang, H.; Zhang, Y.; Pan, J.; Yin, J.; Bakr, O. M.; Mohammed, O. F., Room-temperature engineering of all-inorganic perovskite nanocrsytals with different dimensionalities. *Chemistry of Materials* **2017,** *29* (21), 8978-8982.
10. Tsai, H.; Nie, W.; Blancon, J.-C.; Stoumpos, C. C.; Asadpour, R.; Harutyunyan, B.; Neukirch, A. J.; Verduzco, R.; Crochet, J. J.; Tretiak, S., High-efficiency two-dimensional Ruddlesden–Popper perovskite solar cells. *Nature* **2016,** *536* (7616), 312.
11. Yuan, M.; Quan, L. N.; Comin, R.; Walters, G.; Sabatini, R.; Voznyy, O.; Hoogland, S.; Zhao, Y.; Beauregard, E. M.; Kanjanaboos, P., Perovskite energy funnels for efficient light-emitting diodes. *Nature nanotechnology* **2016,** *11* (10), 872.
12. Yin, J.; Maity, P.; De Bastiani, M.; Dursun, I.; Bakr, O. M.; Brédas, J.-L.; Mohammed, O. F., Molecular behavior of zero-dimensional perovskites. *Science advances* **2017,** *3* (12), e1701793.
13. Zhang, Y.; Saidaminov, M. I.; Dursun, I.; Yang, H.; Murali, B.; Alarousu, E.; Yengel, E.; Alshankiti, B. A.; Bakr, O. M.; Mohammed, O. F., Zero-dimensional Cs_4PbBr_6 perovskite nanocrystals. *The journal of physical chemistry letters* **2017,** *8* (5), 961-965.
14. Babayigit, A.; Thanh, D. D.; Ethirajan, A.; Manca, J.; Muller, M.; Boyen, H.-G.; Conings, B., Assessing the toxicity of Pb-and Sn-based perovskite solar cells in model organism Danio rerio. *Scientific reports* **2016,** *6*, 18721.
15. Noel, N. K.; Stranks, S. D.; Abate, A.; Wehrenfennig, C.; Guarnera, S.; Haghighirad, A.-A.; Sadhanala, A.; Eperon, G. E.; Pathak, S. K.; Johnston, M. B., Lead-free organic–inorganic tin halide perovskites for photovoltaic applications. *Energy & Environmental Science* **2014,** *7* (9), 3061-3068.
16. Huang, L.-y.; Lambrecht, W. R., Electronic band structure, phonons, and exciton binding energies of halide perovskites $CsSnCl_3$, $CsSnBr_3$, and $CsSnI_3$. *Physical Review B* **2013,** *88* (16), 165203.
17. Jellicoe, T. C.; Richter, J. M.; Glass, H. F.; Tabachnyk, M.; Brady, R.; Dutton, S. n. E.; Rao, A.; Friend, R. H.; Credgington, D.; Greenham, N. C., Synthesis and optical properties of lead-

free cesium tin halide perovskite nanocrystals. *Journal of the American Chemical Society* **2016,** *138* (9), 2941-2944.
18. Park, B. W.; Philippe, B.; Zhang, X.; Rensmo, H.; Boschloo, G.; Johansson, E. M., Bismuth based hybrid perovskites $A_3Bi_2I_9$ (A: methylammonium or cesium) for solar cell application. *Advanced materials* **2015,** *27* (43), 6806-6813.
19. Fan, Q.; Biesold-McGee, G. V.; Xu, Q.; Pan, S.; Peng, J.; Ma, J.; Lin, Z., Lead-Free Halide Perovskite Nanocrystals: Crystal Structures, Synthesis, Stabilities, and Optical Properties. *Angewandte Chemie International Edition* **2019,** 10.1002, 201904862.
20. Dahl, J. C.; Osowiecki, W. T.; Cai, Y.; Swabeck, J. K.; Bekenstein, Y.; Asta, M.; Chan, E. M.; Alivisatos, A. P., Probing the Stability and Band Gaps of $Cs_2AgInCl_6$ and $Cs_2AgSbCl_6$ Lead-Free Double Perovskite Nanocrystals. *Chemistry of Materials* 2019, 31(9), 3134-3143.
21. Locardi, F.; Cirignano, M.; Baranov, D.; Dang, Z.; Prato, M.; Drago, F.; Ferretti, M.; Pinchetti, V.; Fanciulli, M.; Brovelli, S., Colloidal synthesis of double perovskite $Cs_2AgInCl_6$ and Mn-doped $Cs_2AgInCl_6$ nanocrystals. *Journal of the American Chemical Society* **2018,** *140* (40), 12989-12995.
22. Greul, E.; Petrus, M. L.; Binek, A.; Docampo, P.; Bein, T., Highly stable, phase pure $Cs_2AgBiBr_6$ double perovskite thin films for optoelectronic applications. *Journal of Materials Chemistry A* **2017,** *5* (37), 19972-19981.
23. Jun, T.; Sim, K.; Iimura, S.; Sasase, M.; Kamioka, H.; Kim, J.; Hosono, H., Lead-Free Highly Efficient Blue-Emitting $Cs_3Cu_2I_5$ with 0D Electronic Structure. *Advanced Materials* **2018,** *30* (43), 1804547.
24. Roccanova, R.; Yangui, A.; Nhalil, H.; Shi, H.; Du, M.-H.; Saparov, B., Near-Unity Photoluminescence Quantum Yield in Blue-Emitting $Cs_3Cu_2Br_{5-x}$ I x (0≤ x≤ 5). *ACS Applied Electronic Materials* **2019,** 1(3), 269-274.
25. Li, T.; Mo, X.; Peng, C.; Lu, Q.; Qi, C.; Tao, X.; Ouyang, Y.; Zhou, Y., Distinct green electroluminescence from lead-free CsCuBr2 halide micro-crosses. *Chemical Communications* **2019,** *55* (31), 4554-4557.
26. Brennan, M. C.; Draguta, S.; Kamat, P. V.; Kuno, M., Light-induced anion phase segregation in mixed halide perovskites. *ACS Energy Letters* **2017,** *3* (1), 204-213.
27. Jiang, H.; Rühle, M.; Lavernia, E., On the applicability of the x-ray diffraction line profile analysis in extracting grain size and microstrain in nanocrystalline materials. *Journal of materials research* **1999,** *14* (2), 549-559.
28. Holzwarth, U.; Gibson, N., The Scherrer equation versus the'Debye-Scherrer equation'. *Nature nanotechnology* **2011,** *6* (9), 534.
29. Liu, H.; Xie, J.; Liu, P.; Dai, B., Effect of Cu^+/Cu^{2+} ratio on the catalytic behavior of anhydrous nieuwland catalyst during dimerization of acetylene. *Catalysts* **2016,** *6* (8), 120.
30. ASPLUND, M.; JAGNER, S., Crystal Structure of bis-(tetraethylammonium) di-mu-bromo-dibromodicuprate (I),[N-$(C_2H_5)_4]_2$ $[Cu_2Br_4]$. *Acta Chem. Scand. A* **1984,** *38* (2).
31. Haddad, S.; Willett, R. D., Dimeric Cu (I) Bromide Species Consisting of Two Edge-Shared Tetrahedra: Crystal Structure of $(C_8H_{14}N2)_2Cu_2Br_6$. *Inorganic chemistry* **2001,** *40* (4), 809-811.
32. Petrov, A. A.; Khrustalev, V. N.; Zubavichus, Y. V.; Dorovatovskii, P. V.; Goodilin, E. A.; Tarasov, A. B., Synthesis and crystal structure of a new hybrid methylammonium iodocuprate. *Mendeleev Communications* **2018,** *28* (3), 245-247.
33. Murphy, J. E.; Beard, M. C.; Norman, A. G.; Ahrenkiel, S. P.; Johnson, J. C.; Yu, P.; Mićić, O. I.; Ellingson, R. J.; Nozik, A. J., PbTe colloidal nanocrystals: synthesis, characterization, and multiple exciton generation. *Journal of the American Chemical Society* **2006,** *128* (10), 3241-3247.
34. Jain, A.; Ong, S. P.; Hautier, G.; Chen, W.; Richards, W. D.; Dacek, S.; Cholia, S.; Gunter, D.; Skinner, D.; Ceder, G., Commentary: The Materials Project: A materials genome approach to accelerating materials innovation. *Apl Materials* **2013,** *1* (1), 011002.
35. Luo, J.; Wang, X.; Li, S.; Liu, J.; Guo, Y.; Niu, G.; Yao, L.; Fu, Y.; Gao, L.; Dong, Q., Efficient and stable emission of warm-white light from lead-free halide double perovskites. *Nature* **2018,** *563* (7732), 541.
36. Halcrow, M. A., Jahn–Teller distortions in transition metal compounds, and their importance in functional molecular and inorganic materials. *Chemical Society Reviews* **2013,** *42* (4), 1784-1795.
37. Yuan, Z.; Zhou, C.; Tian, Y.; Shu, Y.; Messier, J.; Wang, J. C.; Van De Burgt, L. J.; Kountouriotis, K.; Xin, Y.; Holt, E., One-dimensional organic lead halide perovskites with efficient bluish white-light emission. *Nature communications* **2017,** *8*, 14051.
38. Zhou, C.; Lin, H.; Tian, Y.; Yuan, Z.; Clark, R.; Chen, B.; van de Burgt, L. J.; Wang, J. C.; Zhou, Y.; Hanson, K., Luminescent zero-dimensional organic metal halide hybrids with near-unity quantum efficiency. *Chemical science* **2018,** *9* (3), 586-593.
39. Fisher, B. R.; Eisler, H.-J.; Stott, N. E.; Bawendi, M. G., Emission intensity dependence and single-exponential behavior in single colloidal quantum dot fluorescence lifetimes. *The Journal of Physical Chemistry B* **2004,** *108* (1), 143-148.
40. Yakunin, S.; Benin, B. M.; Shynkarenko, Y.; Nazarenko, O.; Bodnarchuk, M. I.; Dirin, D. N.; Hofer, C.; Cattaneo, S.; Kovalenko, M. V., High-resolution remote thermometry and thermography using luminescent low-dimensional tin-halide perovskites. *Nature Materials* **2019,** 18, 846-852.
41. Kim, Y.-E.; Kim, J.; Park, J. W.; Park, K.; Lee, Y., σ-Complexation as a strategy for designing copper-based light emitters. *Chemical Communications* **2017,** *53* (19), 2858-2861.
42. Dias, H. R.; Diyabalanage, H. V.; Rawashdeh-Omary, M. A.; Franzman, M. A.; Omary, M. A., Bright phosphorescence of a trinuclear copper (I) complex: luminescence thermochromism, solvatochromism, and "concentration luminochromism". *Journal of the American Chemical Society* **2003,** *125* (40), 12072-12073.
43. Nedelcu, G.; Protesescu, L.; Yakunin, S.; Bodnarchuk, M. I.; Grotevent, M. J.; Kovalenko, M. V., Fast anion-exchange in highly luminescent nanocrystals of cesium lead halide perovskites (CsPbX3, X= Cl, Br, I). *Nano Letters* **2015,** *15* (8), 5635-5640.
44. Protesescu, L.; Yakunin, S.; Bodnarchuk, M. I.; Krieg, F.; Caputo, R.; Hendon, C. H.; Yang, R. X.; Walsh, A.; Kovalenko, M. V., Nanocrystals of cesium lead halide perovskites ($CsPbX_3$, X= Cl, Br, and I): novel optoelectronic materials showing bright emission with wide color gamut. *Nano letters* **2015,** *15* (6), 3692-3696.
45. Harris, R. K.; Becker, E. D.; Cabral de Menezes, S. M.; Goodfellow, R.; Granger, P., NMR nomenclature: nuclear spin properties and conventions for chemical shifts. IUPAC Recommendations 2001. International Union of Pure and Applied Chemistry. Physical Chemistry Division. Commission on Molecular Structure and Spectroscopy. *Magnetic Resonance in Chemistry* **2002,** *40* (7), 489-505.

TOC

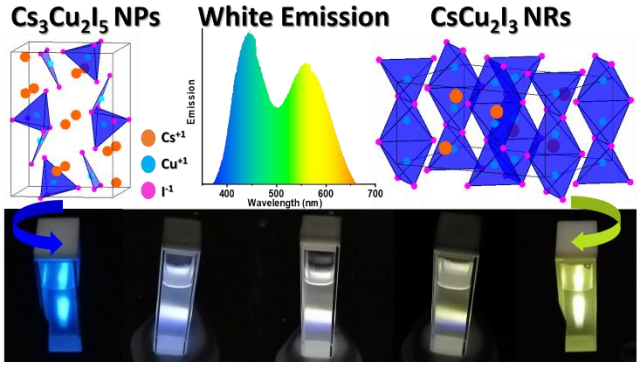
Cs3Cu2I5 NPs
White Emission
CsCu2I3 NRs
Cs+1
Cu+1
I-1
Emission
400
500
600
700
Wavelength (nm)